Research Article | Vol. 33, No. 14 / 14 Jul 2025 / Optics Express 28935
Optics EXPRESS

Chirped pulse waveguide amplifier

ALEXANDER RUDENKOV,[1,*] VLADIMIR L. KALASHNIKOV,[1] MAKSIM DEMESH,[1] NIKOLAI TOLSTIK,[1] EVGENI SOROKIN,[2,3] AND IRINA T. SOROKINA[1,3]

[1]*Department of Physics, Norwegian University of Science and Technology, Høgskoleringen 5, N-7491 Trondheim, Norway*
[2]*Photonics Institute, Vienna University of Technology, Gußshausstr. 27/387, 1040 Vienna, Austria*
[3]*ATLA Lasers AS, Richard Birkelands vei 2B, 7034 Trondheim, Norway*
[*]*alexander.rudenkov@ntnu.no*

Abstract: We introduce the first ultrafast Cr:ZnS amplifier in a 34-mm-long depressed-cladding waveguide with a cross-section of up to 50 μm and an excellent output beam quality of $M^2 \sim 1.2$. In a chirped pulse amplification scheme incorporating a Chirped Volume Bragg Grating stretcher/compressor, the amplifier achieves an optical gain of 75 over 15 mm, corresponding to a 12 dB/cm gain coefficient. The amplifier delivers 2.35 W of average output power in a single pass, with the amplified pulses being compressed to 235 fs. Furthermore, our numerical 3D model, which accounts for the spatial profiles of both the pump and the seed beams, reveals and describes experimental observation of what we believe to be a novel phenomenon: multimode relaxation to the fundamental transverse mode in a large-mode-area (LMA) waveguide, occurring without degradation of the effective mode volume or amplification efficiency. We also demonstrate that without stretching, the waveguided propagation in a non-centrosymmetric Cr:ZnS medium enables effective generation of multiple harmonics even for the relatively long 100-fs seed pulses, making an integrated carrier-envelope phase stabilization using 2f-3f or 3f-4f schemes within reach.

© 2025 Optica Publishing Group under the terms of the Optica Open Access Publishing Agreement

1. Introduction

The mid-infrared (mid-IR) wavelength range, often referred to as the "molecular fingerprint" region, and specifically the range between 2 and 5 μm, is characterized by strong fundamental and overtone rovibrational absorption bands of atmospheric constituents, vapors, and gases such as carbon monoxide and dioxide, methane, ammonia, NOx, and others. The key advantage of ultrashort-pulsed solid-state lasers is their ability to spectrally cover this broad wavelength range, either by generating an ultrashort pulse spectrum that simultaneously encompasses all these absorption bands or through rapid laser tuning. This capability makes ultrabroadband Cr^{2+}-doped II-VI compound-based lasers [1–5] particularly attractive for various environmental and climate-change-related sensing applications [6–8].

This class of lasers has matured and stands out with unparalleled performance, rivaled only by $Ti^{3+}:Al_2O_3$ lasers. These lasers achieve the broadest bandwidth among all existing solid-state lasers—up to 45% of the central wavelength—and can reach power levels in the tens of watts in the continuous-wave regime, with a notable example being a 140 W Cr:ZnSe laser system [9,10]. Additionally, they generate femtosecond pulses with terawatt-level peak powers [11] and enable free-space frequency comb generation [4,12–14], including carrier-envelope phase (CEP) stabilized Cr^{2+}:ZnS lasers [15]. In bulk format, Cr^{2+}:ZnS supports high-power, broadly tunable, and few-cycle ultrafast laser operation, including frequency comb generation [4,9,16,17], even in the directly diode-pumped configurations [13,18]. These gain media enable the generation of several-watt-level output powers in direct femtosecond amplification [19], and up to 27 W from a spinning-ring Cr:ZnSe amplifier [20]. Advances in power scaling have enabled nonlinear

#558940 https://doi.org/10.1364/OE.558940
Journal © 2025 Received 6 Feb 2025; revised 5 Jun 2025; accepted 5 Jun 2025; published 30 Jun 2025

Optics EXPRESS

frequency conversion to generate mid-IR radiation covering the entire "molecular fingerprint" region from 3 to 18 μm [9,13,21].

Naturally, there is currently a growing interest in the community toward integrating ultrashort-pulse laser technology, in general, and this specific technology, in particular, with photonic circuits. Such integration would enable scalability, stability, and robustness while also reducing cost and size by at least three orders of magnitude. Moreover, given the critical importance of this wavelength range above 2 μm, it would profoundly impact industry and everyday life. Over the past two decades, there has been a surge of research in silicon photonics, with fields such as Si optical interconnects and other passive devices maturing to the point of industrial adoption, including applications in mega-scale data centers operated by major research and technology companies like Intel. However, light emitters remain a significant challenge, as silicon's indirect bandgap prevents the direct fabrication of lasers or LEDs, even through doping. As a result, demonstrated silicon photonic systems still rely on external light sources, such as VCSELs [22].

Interestingly, Cr^{2+}-doped ZnS lasers [18,23] offer a promising route for direct integration with silicon photonics, as ZnS is one of the few semiconductors that are lattice-matched to Si, enabling seamless integration. Being lattice matched to Si, ZnS is one of the prospective materials recently identified for the future Si-photonics-based quantum technology platform [24]. Recently, using molecular beam epitaxy (MBE), we have demonstrated the first lithographically fabricated thin-film Cr^{2+}:ZnS waveguide [25,26]. Furthermore, the operating wavelength range of Cr^{2+}:ZnS (2–3.1 μm) [3,27] falls within the transparency window of Si, making it particularly well-suited for ultrashort-pulse silicon photonics. An additional advantage is that the Cr^{2+}:ZnS emission range (2–3 μm) lies beyond the two-photon absorption threshold of Si (below 2.1 μm), reducing nonlinear losses and further enhancing its compatibility with silicon-based photonic systems.

The laser writing technique serves as an alternative to lithography for the fabrication of waveguides. In 2004, two research groups independently reported the inscription of depressed cladding waveguides for future laser applications—first in lithium fluoride (LiF) with F_2-color centers [28] and then in Ti^{3+}:Al_2O_3 crystal [29]. Following these conceptual studies, A. Okhrimchuk et al. demonstrated the first depressed cladding waveguide laser in a Nd^{3+}-doped YAG crystal [30]. A decade later, J.R. Macdonald et al. developed waveguide structures in polycrystalline Cr:ZnS [31]. The first polycrystalline channel waveguide laser was realized by Ya-Pei Peng et al. [32], using femtosecond laser helical writing in a 2 mm thick Cr^{2+}:ZnS sample. The tendency of scattering losses to decrease with wavelength as $1/\lambda^4$ makes waveguide laser writing particularly attractive for mid-IR active media such as Cr^{2+}:ZnS [31,33,34], Cr^{2+}:ZnSe [35–38], Fe^{2+}:ZnSe [37,39], as well as Tm^{3+}:ZBLAN [40] and Ho^{3+}:YAG [41,42]. Further optimization of waveguide parameters led to power scaling in various systems, reaching 5.6 W output power in Yb^{3+}:YAG [43] and 5.1 W in Cr^{2+}:ZnSe, albeit in a multimode regime, with an impressive slope efficiency of 41% [37]. A significant milestone was achieved when N. Tolstik et al. reported the first single-crystal single-mode Cr^{2+}:ZnS depressed cladding buried waveguide laser, fabricated by femtosecond laser writing. This laser delivered 150 mW of average power at 2272 nm with an 11% slope efficiency [33]. The most recent milestone in the development of a new class of miniature, ultra-broadband lasers and sensors was the demonstration of the first all-laser-microprocessed Cr^{2+}:ZnS waveguide laser [34], in which both the waveguide and antireflection coatings were fabricated via laser writing. However, all these achievements were made in relatively short waveguides (typically within 1 cm in length). The first attempt to achieve amplification in a 7 mm-long, 90 μm wide Cr:ZnSe waveguide resulted in an internal gain factor of 5.375, with 430 mW of average output power and a 3.4% power-added optical efficiency [44]. The latest step toward integrated photonics was the demonstration of a Ti^{3+}:Al_2O_3-on-insulator waveguide amplifier [45]. However, even in this case, the waveguide amplifier length was limited

Optics EXPRESS

to 8 mm, which remains a typical constraint for all waveguide lasers and amplifiers reported so far.

In this work, we present a proof-of-principle demonstration of what is, to the best of our knowledge, the first chirped-pulse amplification (CPA) [46] in a relatively long (34 mm) depressed cladding Cr^{2+}:ZnS waveguide, substantially exceeding the typical few-millimeter propagation lengths. This result provides clear evidence of true waveguiding behavior, achieving a high gain of up to 75, an average output power of 2.35 W, and the generation of ultrashort pulses with near-single-mode beam quality. We obtained nearly transform-limited 235 fs pulses at 2.35 μm wavelength in a compact CPA configuration featuring an 'all-in-one' stretcher/compressor based on a single-volume Bragg grating. Finally, we demonstrate the possibility of simultaneous pulse generation at harmonic wavelengths within our waveguide, analogous to the phenomenon first reported in Ref. [47]. This advancement paves the way toward a compact waveguide source with carrier-envelope phase stabilization.

2. Experimental implementation

The schematic of the experimental setup is shown in Fig. 1. As a seed pulse source, we used a Kerr-lens mode-locked Cr^{2+}:ZnS laser, similar to the 70 MHz laser described in [48,49]. The laser was pumped through dichroic mirrors (DM) by a low-noise 1610 nm Er:fiber laser. Intracavity dispersion compensation was achieved using broadband chirped mirrors (CM). The seed laser exhibited a FWHM spectral width of 106 nm at a central wavelength of 2336 nm, corresponding to a pulse duration of approximately 85 fs (see Supplement 1, Fig. S1). These spectral characteristics enabled optimal filling of the chirped volume Bragg grating (CVBG) reflection band. A Faraday isolator (FI) was placed after the seed laser to prevent feedback from the amplifier section due to the uncoated Cr:ZnS facets.

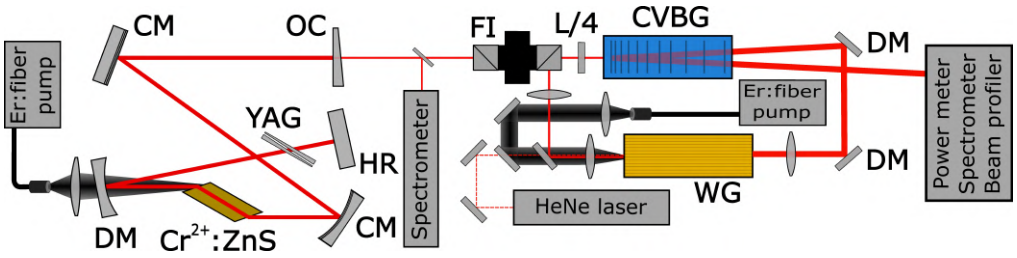

Fig. 1. Experimental setup: CM-chirped mirror, OC-output coupler, FI-Faraday isolator, L/4-quarter wave plate, CVBG-chirped volume Bragg grating, YAG-wedges for dispersion adjustment, HR-highly reflective mirror, DM-dichroic mirror, WG- Cr^{2+}:ZnS polycrystalline active element with inscribed waveguides.

In this experiment, we primarily focused on investigating the power/energy gain performance of the waveguides. The chirped seed pulses had a duration of approximately 500 ps, with a 100 nm spectral width centered at 2.35 μm, provided by the specially designed chirped volume Bragg grating (CVBG) from OptiGrate. The reflection coefficient of the CVBG was about 60% (the CVBG reflectance spectrum is shown in Supplement 1, Fig. S2). This type of CVBG can be effectively used as a stretcher unit, and the relatively long pulse duration helps to eliminate most nonlinear effects that could arise during amplification. Next, the laser beams from the seed, pump, and red guide laser were focused onto the input face of the active element. The average power of the seed laser pulses incident on the waveguide was approximately 100 mW. For waveguide pumping, we used an Er:fiber laser (15 W at 1550 nm, IPG Photonics). Compression of the amplified pulses was achieved through reflection from the back side of the same CVBG and,

Optics EXPRESS

for comparison, using a diffraction grating compressor with 600 grooves/mm. Using the same CVBG for both stretching and compressing the amplified pulses makes the system more compact.

To characterize the amplified radiation parameters, we used an Ophir 30 (150) A-BB-18 power meter, Ocean Optics SD2000 spectrometer (490–1150 nm), APE Berlin waveScan spectrometer (800–2600 nm), and a Thorlabs BP109-IR2 slit-scanning beam profiler (1000–2700 nm).

For the direct laser writing of waveguides, we used a picosecond Ho:YAG MOPA laser system (ATLA Lasers AS) operating at a central wavelength of 2090 nm. We fabricated 31 circular waveguides with diameters ranging from 20 to 50 μm, inscribed in a 34-mm-long polycrystalline Cr^{2+}:ZnS sample (Cr^{2+} concentration: $2.9 \cdot 10^{18}$ cm^{-3}) using an objective with NA = 0.85. The inscription was performed in single-pulse modification mode, where a single laser pulse formed each defect without overlap. The spacing between consecutive defects along the optical axis of the inscribing beam was 3 and 4 μm [50]. This approach is equivalent to free-form 3D printing, providing a high degree of flexibility in waveguide design.

3. Results and analysis

3.1. Femtosecond chirped pulse waveguide amplifier

During the experiment, we measured the dependence of the average power of the amplified pulses on the incident pump power for each waveguide. To eliminate the influence of the uncoated facets of the active element and variations in coupling conditions, the gain factor was estimated by comparing the average power of the seed pulses measured at the same position at the waveguide output after the dichroic mirrors with and without applied pump power (the Γ-coefficient).

The experimental results are categorized into four groups based on the corresponding waveguide diameter (see Table 1). The highest average output power, gain factor, and beam quality were achieved with 50 μm waveguides (for a detailed description, see Supplement 1, Experiment).

Table 1. Output characteristics of waveguide amplifiers

Waveguide diameter	Gain factor	Maxumum power	Optical efficiency
50 μm	75	2.35 W	16.2%
50 μm [a]	29	2.05 W	14.3%
40 μm	68	2.04 W	14.0%
30 μm	6.5	0.3 W	1.8%
20 μm	5.01	0.23 W	1.26%

[a]Waveguide amplifier of sub-ps pulses.

As evident from the experimental data, the gain factors achieved with large cross-section waveguide amplifiers can significantly exceed those of comparable Cr:ZnS amplifiers based on bulk crystals [51–53]. The difference is even more striking is one considers the fact that the observed input-output gain is reduced by 15% Fresnel losses on each uncoated surface, plus coupling and propagation losses in the yet non-optimized system, which we estimate to amount to about 57%. For instance, in a 50 μm waveguide, the total gain factor of 23.5 (2.35 W / 100 mW) corresponded to 75× optical gain. This gain was achieved in the first 15 mm of the crystal ($2.5l_{abs}$), where over 90% of pump radiation was absorbed (see also Fig. 6(e)), corresponding to over 12 dB/cm gain coefficient. This is possible due to the extended interaction length with the high-intensity pump radiation in the waveguide. Without a waveguide, the same beam size would have had only 2 mm Raleigh range in the crystal. We thus conclude that waveguide amplifiers enable significantly higher gain factors than bulk amplifiers of the same class.

Optics EXPRESS

The measured output beam quality parameter M^2 factor of 1.13x1.25 (in vertical and horizontal planes, respectively) and 2D beam profile are shown in Fig. 2.

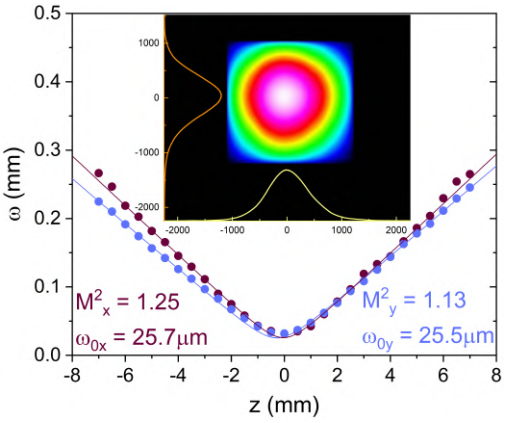

Fig. 2. M^2 factor measurement results and 2D output beam profile.

Figure 3(a) shows spectra of the seed, amplified pulse, and amplified spontaneous emission (ASE) in the waveguide amplifier. Following our proposed concept, we used the same chirped volume Bragg grating (CVBG) for both pulse stretching and compression by reflecting the pulse from the opposite side of the CVBG. The interferometric autocorrelation obtained in this case is shown in Fig. 3(b), illustrating a compressed pulse duration of approximately 235 fs, assuming a $sinc^2$ temporal pulse shape, which corresponds to the nearly rectangular pulse spectrum after passing through the CVBG. For comparison, we also implemented temporal pulse compression using a diffraction grating (DG) compressor. Figure 3(c) shows the intensity autocorrelation (AC) traces obtained from the measured interferometric ACs for both the CVBG and DG compressors, along with the AC of transform-limited pulses calculated from the pulse spectrum. The AC trace width of the CVBG-compressed pulses (314 fs) is comparable to the AC width of the transform-limited pulses (250 fs) and is significantly narrower than that of the grating-compressed pulses (1560 fs). We attribute this difference to the presence of significant third- and higher-order dispersion in the grating compressor compared to the CVBG stretcher.

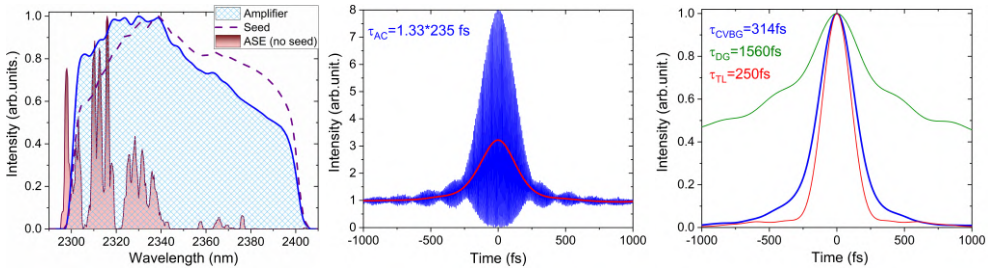

(a) (b) (c)

Fig. 3. Chirped pulse waveguide amplifier: seed, ASE and amplified pulse spectra (a), interferometric autocorrelation trace (AC) of CVBG compressed pulses (b), intensity autocorrelation traces of compressed pulses: CVBG compressor (blue), diffraction grating compressor (green) and calculated AC for transform-limited pulses (red) (c).

Optics EXPRESS

3.2. Nonlinear harmonic generation in a femtosecond pulse waveguide amplifier

Chirped-pulse amplification with reduced nonlinear effects is not the only possible use for an ultrashort pulse amplifier. The enhanced nonlinearity in a waveguide, resulting from precise and strong mode control, enables numerous applications. For instance, it facilitates the generation of an ultra-broadband supercontinuum directly from the fiber amplifier [12] or the generation of phase-synchronized frequency combs at fundamental and harmonic wavelengths. This topic has garnered considerable attention in the ultrafast optics community and has been extensively explored both theoretically and experimentally in polycrystalline bulk amplifiers [54], laying the groundwork for the development of carrier-envelope phase (CEP)-controlled [55] multi-octave-spanning spectra.

In our study, we experimentally investigated the simultaneous generation of optical harmonics and femtosecond pulse amplification in a waveguide amplifier. For this purpose, the CVBG was removed from the signal beam path. Table 1 presents the results (50 μm [a]), corresponding to the experiment with non-stretched pulses.

It should be noted that the results for the amplification of chirped and femtosecond pulses (50 μm and 50 μm [a] in Table 1) were obtained using different waveguides, #1 and #28, respectively. In the chirped-pulse mode, the average power of waveguide #28 reached 2.11 W, with an optical gain factor of 57 and a power-added optical efficiency of 16.1% (for more details, see Supplement 1, Fig. S3).

The femtosecond seed pulse acquired a negative chirp in the isolator and polarizing optics, entering the gain medium with ~150 fs duration. After 20–25 mm propagation, the chirp is compensated by the 130 fs^2/mm positive dispersion in the gain medium, then the pulse is stretched again to about 100 fs duration. In a non-centrosymmetric ZnS crystal, the high second-order nonlinearity [3] causes generation of the second [47] and, with short and energetic pulses, also higher-order harmonics [15], enhanced by the random quasi-phase matching [56] in the ceramic samples. We have been able to observe the generation of the 2nd, 3rd, and 4th harmonics Fig. 4, which were co-propagating in the waveguide (Fig. 5). With shorter seed and optimized dispersion pre-compensation we expect to observe also pulse spectral broadening [15], and much broader harmonic spectra, eventually opening the path to integrated carrier-envelope phase control using 2f-3f or 3f-4f schemes [15].

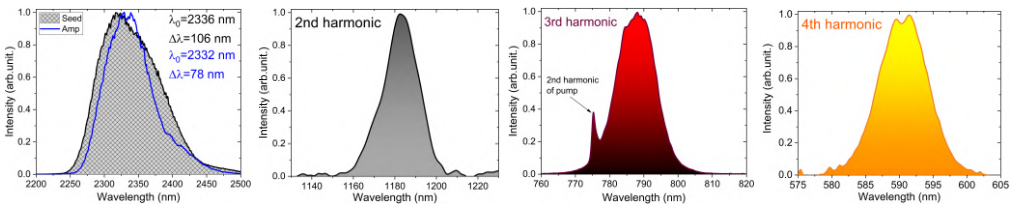

Fig. 4. Waveguide amplifier in sub-ps regime: seed, amplified pulse spectra (a) and harmonics spectra: 2nd harmonic (b), 3rd harmonic (c), 4th harmonic (d).

3.3. Theoretical analysis

Our experimental findings demonstrate highly effective amplification in a multimode waveguide with an output beam spatial quality close to that of a single-mode one. This implies optimizing the mode spectrum, overlap, and mode crosstalk to maintain $M^2 \approx 1$ while maximizing the gain coefficient. This objective is analogous to mode control in large-mode-area fibers, which enables energy scaling in fiber lasers and oscillators [57,58]. To investigate the waveguiding properties

Optics EXPRESS

Fig. 5. A photo of the 4th harmonic generation in waveguide.

of the amplifier, we relied on the three-dimensional model of multimode laser amplification outlined in [59] (for a detailed description, see Supplement 1, Theory).

We note that the waveguides used in this experiment are, in fact, *large-mode-area photonic crystal waveguides* [60,61], schematically illustrated in Fig. 6(a–c). Consequently, their mode structure is influenced by both the large-scale (b, c) and small-scale (a) geometries. However, there is a distinction between low-NA large-mode-area single-mode fibers and the waveguides examined in this study. In our case, the numerical aperture (NA) varies within the range of approximately $0.1 - 0.3$. While these waveguides are multimodal, they still allow for reasonable control of mode quality. Moreover, crystalline waveguides exhibit a more robust structure and are less sensitive to bending and imperfections compared to photonic crystal fibers. Additionally, a significant advantage of both solid-state and fiber waveguides, as power- and nonlinearity-scalable devices for various applications, is their substantial reduction of thermal effects due to the larger surface-to-volume ratio of the mode compared to bulk materials. Approximate calculations indicate that the thermal properties of Cr^{2+}:ZnS, in combination with waveguide technology [27,32], enhance the robustness of the modal structure against thermal lensing (see Supplement 1, Theory).

For modeling, we assume a cylindrical symmetry for the waveguide and a (super-)Gaussian dependence of the refractive index on the radial coordinate, R^{2m} ($m = 1, 2, 3$) (see Supplement, Theory). Thus, the parameter m defines the "sharpness" of the waveguide confining potential and can be expected to increase with w_0 (Fig. 6(b,c)). The parameter δn represents the difference between the refractive index at the waveguide axis, n_1, and at its edge, n_0 (see Fig. 6). The value of δn varies with the waveguide size w_0 such that n_1 approaches the bulk refractive index, n_{core}, as w_0 increases (Fig. 6(b,c)).

Such a design offers a wide range of tools for mode manipulation, including power scaling by mode area and mode synthesis. In our case, one can consider the transition from a thin waveguide (c) to a thick one (b) in parallel with the increase of $\delta n = n_1 - n_0$ and m.

Analyzing the output beam profiles for waveguides with different w_0 (Table 1), along with the measured M^2 factors (Fig. 2), we observe that the unique spatial mode spectrum of each specific waveguide dictates the spatial profile formation of the amplified pulse beam. However, unlike fiber lasers, waveguides feature a well-defined and rigid geometry, as well as a short length. Consequently, the primary factor influencing the quality of the output beam is the coupling conditions of the incident radiation in conjunction with the waveguide's eigenmode spectrum.

Ultimately, this enables the achievement of high spatial beam quality even in large-diameter waveguides, which are inherently multimode in nature (Figs. 2 and 6(d)). The underlying mechanism of power transfer from higher-order modes to the fundamental mode is driven by random mode coupling, similar to the phenomenon reported in [63] under conditions of negligible modal dissipation. In our case, this effect is further enhanced by the presence of a transversely profiled gain, which acts as a soft aperture [64,65].

Nevertheless, intermodal beatings, enhanced by pump-signal coupling, play a significant role in the fine structuring of the effective gain within the initial section of the waveguide, as illustrated in Fig. 6(e). This figure shows the evolution of the calculated effective gain Γ along

Optics EXPRESS

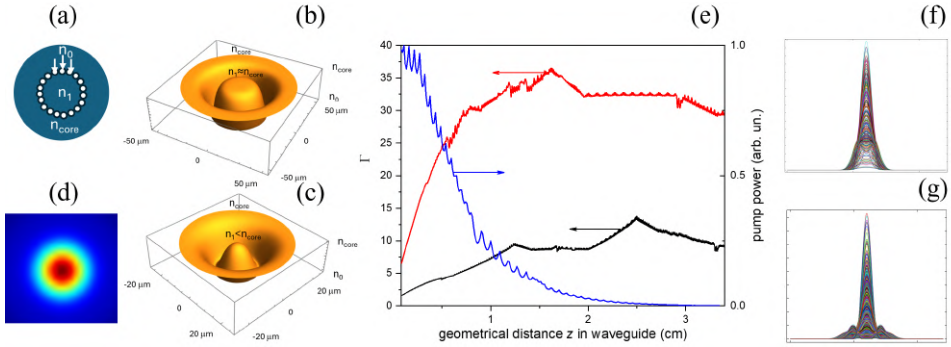

Fig. 6. (a): The holes (shown by the white circles) are manufactured by laser processing inside a bulk ZnS-sample with the refractive index n_{core}; the modified refractive index inside the holes is n_0 and rises to n_1 at the waveguide axis. Since the length of refractive index relaxation is about 10 μm [62], the effective δn and m would be lower for a thin waveguide (c) and larger for a thick one (b). (d): The output mode profile for the red curve parameters of (e) (the dimension is of 100×100 w_T, where $w_T = \sqrt[2(m+1)]{w_0^{2m}/k_0^2 n_0 \delta n}$ is a normalized transverse coordinate and k_0 is a wavenumber). (e): The amplification gain Γ vs. the geometrical distance z of waveguide propagation for m=1 (black curve) and 2 (red), the input pump power is of 12 W (black) and 22 W (red), and the waveguide size w_0 equals 20 (black) and 50 (red) μm; δn =0.003 (black) and 0.021 (red); the blue curve shows the normalized pump power vs. z for the input pump power of 22 W, m = 2, w_0=50 μm, and δn=0.003. (f) and (g): are the accumulated transverse (R) intensity ($|E(z,R)|^2$) profiles for the red and black curves of (e), respectively. The colored lines show the accumulated contribution of the higher-order modes to the output beam profile.

the waveguide axis (z) for two waveguides with $w_0 = 20\mu$m (black curve) and $w_0 = 50$ μm (red) under the experimental conditions described above. The effective gain of the amplified power is defined as

$$\Gamma = \frac{\int_{-x_{min}}^{x_{max}} \int_{-y_{min}}^{y_{max}} |E\,(z,x,y;\,P(z,x,y))|^2\,dxdy}{\int_{-x_{min}}^{x_{max}} \int_{-y_{min}}^{y_{max}} |E\,(z_{out},x,y;\,P(z,x,y)=0)|^2\,dxdy}, \tag{1}$$

where $E\,(z,x,y;\,P(z,x,y))$ in the numerator represents the amplifying field evolving alongside the pump beam $P(z,x,y)$. The transverse coordinates are denoted as x and y, with cylindrical symmetry assumed, where $R = \sqrt{x^2+y^2}$ is the radial coordinate. The power of the amplifying field in the numerator corresponds to the field at the waveguide output (z_{out}=3.4 cm) after propagation in the absence of a pump. Both the seed and pump beams are Gaussian at the input, with equal beam sizes of 16 μm. We consider an input stretched seed pulse with a peak power of 2.94 W. The integration limits in Eq. (1) are chosen to be sufficiently large to encompass the entire beam. The blue curve illustrates an example of the evolution of the normalized pump power, given by $\int\int |P(z,x,y)|^2\,dxdy / \int\int |P(0,x,y)|^2\,dxdy$.

Qualitatively, the simulations are in good agreement with the experimental results. However, the following factors can be attributed to some quantitative discrepancies in the Γ value for $w_0 = 50\mu$m. The model assumes perfect cylindrical symmetry, which may result in larger mode volumes and increased mode overlap compared to the experimental waveguides, where slight deviations from circular symmetry are present (see Fig. 2). This deviation could enhance mode crosstalk and lead to earlier gain depletion.

It is important to note that the perfect pump depletion observed in the waveguide (blue curve in Fig. 6(e)) is consistent with experimental results. This observation paves the way for gain scaling through two-sided (counter-propagating) waveguide pumping. Furthermore, waveguided

Optics EXPRESS

field propagation beyond the effective gain region ("passive propagation") leads to accumulated nonlinearity, creating favorable conditions for higher-harmonic generation, as illustrated in Fig. 5. Additionally, our simulations indicate that a stable mode, as shown in Fig. 6(f), is established early in the amplification process (within <2 cm for the given parameters). Consequently, further propagation does not hinder two-sided amplification or the accumulation of nonlinearity in the waveguide amplifier.

The simulations show that increasing the "steepness" index m while simultaneously increasing δn in a "thick" waveguide (Fig. 6(b)) enhances both the gain coefficient and mode quality (Figs. 6(d), (e), and (f)) (red curve) compared to Figs. 6(e) and (g) (black)). It can be conjectured that increasing the waveguide size reduces mode overlap as the m-index and δn increase [66]. As a result, inter-mode crosstalk is reduced, leading to improved output mode quality. At the same time, the increase in the total mode volume, which is approximately proportional to the number of modes $\approx (2\pi w_0/\lambda)^2(n_1^2 - n_0^2)$ [67], contributes to the Γ-increase.

4. Conclusion and outlook

In this work, we propose and implement the concept of an ultrafast laser system based on a waveguide amplifier fabricated using the laser writing method. Laser writing of waveguides provides a level of design flexibility that is difficult to achieve with other techniques, such as adjusting the diameter or even the numerical aperture (NA) of the waveguide along the propagation direction. The enhanced flexibility of laser-written waveguides enables power and energy scaling through large waveguide cross-sections while maintaining excellent spatial beam quality and good overlap between the pump and amplified pulse beams along the active medium. By fabricating a long waveguide, we can integrate both the gain and nonlinear-optical conversion stages for subsequent comb stabilization into a single element. The long, truly waveguide propagation allows for harmonic generation at lower power than bulk systems, thereby enabling all-in-one generation, amplification, and nonlinear optical conversion of ultrashort pulses. The novel results obtained in this work are as follows:

- For the first time, to the best of our knowledge, we have employed the concept of chirped pulse amplification in conjunction with a waveguide active medium and an all-in-one, single chirped volume Bragg grating-based stretcher/compressor. This approach provides a high gain of 12 dB/cm and 1.4 W of average output power (2.35 W of uncompressed output power), with the duration of the amplified pulse compressed to 235 fs.

- We experimentally validated the energy/power scaling concept by increasing the waveguide mode area while maintaining the excellent spatial quality of the output beam (similar to large-mode-area (LMA) fibers). By using a large cross-section multimode Cr^{2+}:ZnS waveguide, we achieved gain factors up to 75 in a single pass, with an average output power of 2.35 W (directly from the waveguide) and excellent output beam quality (M^2=1.13x1.25). To the best of our knowledge, this is the first demonstration of a waveguide amplifier in a crystalline active medium operating with such high spatial quality of the output beam, comparable to a single Gaussian transverse mode.

- For the first time, to the best of our knowledge, we developed a comparatively long (34 mm) laser-written waveguide in a Cr^{2+}:ZnS gain element, exhibiting true waveguiding properties. These properties offer additional degrees of freedom for experiments with longitudinally graded gain, which can be further exploited when pumping from both sides of the waveguide.

- We developed a 3D waveguide amplifier model that accounts for waveguide effects on both the pump and amplifying spatially profiled beams. The model demonstrates that the interplay between the non-dissipative (transversely graded refractive index) and dissipative

Optics EXPRESS

(transversely graded gain) confining potentials results in the integration of higher-order modes into lower-order ones (spatial mode synthesis or "mode condensation" [68]). This enables more efficient use of the entire gain volume and energy harvesting in multimode waveguides while maintaining good output beam quality.

- For the first time, to the best of our knowledge, we demonstrate optical harmonic generation up to the 4th harmonic, enabled by enhanced nonlinear effects in the amplifying active medium owing to its waveguide nature. By using a comparatively long waveguide, it was possible to organize the amplification of seed pulses in the input section and achieve nonlinear optical conversion with harmonic generation in the output section of the waveguide.

The latter result is of particular interest to the ultrafast laser community. Indeed, the combination of well-developed waveguiding properties with the high nonlinearity characteristic of a non-centrosymmetric active medium like Cr:ZnS [3] provides broad flexibility in the development of ultrafast laser systems. This was demonstrated in our work, both through experiments amplifying strongly chirped pulses (with a duration of about 500 ps) and experiments involving harmonic generation while amplifying weakly chirped pulses with a duration of about 100 fs. Looking into the future, extending this result to even shorter pulses holds the potential to generate octave-spanning, overlapping spectra at the fundamental and harmonic wavelengths, offering a straightforward path to CEP stabilization via the f–2f, 2f-3f or 3f-4f techniques. Such phase-stabilized integrated mid-infrared frequency combs will open up a wide avenue towards quantum shot noise-limited, ultra-sensitive detection directly in the mid-IR.

Funding. Norges Forskningsråd (#303347 (UNLOCK), #326241 (Lammo-3D), #326503 (MIR)); ATLA Lasers AS.

Acknowledgment. The work of AR, VLK, MD, and ITS was supported by NFR projects #303347 (UNLOCK), #326503 (MIR), #326241 (Lammo-3D) and by ATLA Lasers AS.

Disclosures. ES: ATLA Lasers AS (I), ITS: ATLA Lasers AS (I, S).

Author contributions. A.R. designed the experiments and analysis methods, contributed to a laser writing setup, and collected, interpreted, and processed data; V.L.K. developed the mathematical methods, performed the theoretical analysis, and interpreted data; M.D. performed laser inscription of the waveguides, preparation of the sample, and its postprocessing. E.S. designed chirped mirrors. N.T. and E.S. developed a laser writing setup and developed the technological process for waveguide writing. I.T.S. developed the experiment and dispersion management concept and guided and supervised the project.

A.R., V.L.K., and I.T.S. wrote and edited the manuscript; M.D., N.T., and E.S. provided the revisions. All the authors were involved in discussing and interpreting the results.

Data availability. Data underlying the results presented in this paper are not publicly available at this time but may be obtained from the authors upon reasonable request.

Supplemental document. See Supplement 1 for supporting content.

References

1. L. DeLoach, R. Page, G. Wilke, *et al.*, "Transition metal-doped zinc chalcogenides: spectroscopy and laser demonstration of a new class of gain media," IEEE J. Quantum Electron. **32**(6), 885–895 (1996).
2. R. Page, K. Schaffers, L. DeLoach, *et al.*, "Cr2+-doped zinc chalcogenides as efficient, widely tunable mid-infrared lasers," IEEE J. Quantum Electron. **33**(4), 609–619 (1997).
3. I. T. Sorokina, "Cr2+-doped II–VI materials for lasers and nonlinear optics," Opt. Mater. **26**(4), 395–412 (2004).
4. I. T. Sorokina and E. Sorokin, "Femtosecond Cr2+-based lasers," IEEE J. Sel. Top. Quantum Electron. **21**(1), 273–291 (2015).
5. S. B. Mirov, V. V. Fedorov, D. Martyshkin, *et al.*, "Progress in Mid-IR lasers based on Cr and Fe-doped II–VI chalcogenides," IEEE J. Sel. Top. Quantum Electron. **21**(1), 292–310 (2015).
6. V. Girard, R. Farrenq, E. Sorokin, *et al.*, "Acetylene weak bands at 2.5 μm from intracavity Cr:ZnSe laser absorption observed with time-resolved fourier transform spectroscopy," Chem. Phys. Lett. **419**(4-6), 584–588 (2006).
7. E. Sorokin, I. T. Sorokina, J. Mandon, *et al.*, "Sensitive multiplex spectroscopy in the molecular fingerprint 2.4 μm region with a Cr2+:ZnSe femtosecond laser," Opt. Express **15**(25), 16540–16545 (2007).
8. B. Bernhardt, E. Sorokin, P. Jacquet, *et al.*, "Mid-infrared dual-comb spectroscopy with 2.4μm Cr2+:ZnSe femtosecond lasers," Appl. Phys. B **100**(1), 3–8 (2010).

Optics EXPRESS

9. S. B. Mirov, I. S. Moskalev, S. Vasilyev, *et al.*, "Frontiers of mid-IR lasers based on transition metal doped chalcogenides," IEEE J. Sel. Top. Quantum Electron. **24**(5), 1–29 (2018).
10. I. Moskalev, S. Mirov, M. Mirov, *et al.*, "140 W Cr:ZnSe laser system," Opt. Express **24**(18), 21090–21104 (2016).
11. X. Lu, X. Wang, J. Fan, *et al.*, "Terawatt-level 2.4-μm pulses based on Cr:ZnS chirped pulse amplification," Optica **10**(11), 1567–1570 (2023).
12. I. T. Sorokina, V. V. Dvoyrin, N. Tolstik, *et al.*, "Mid-IR ultrashort pulsed fiber-based lasers," IEEE J. Sel. Top. Quantum Electron. **20**(5), 99–110 (2014).
13. N. Nagl, *A New Generation of Ultrafast Oscillators for Mid-Infrared Applications*, Springer Theses (Springer Cham, 2022), 1st ed. Published: 02 February 2022, Hardcover ISBN: 978-3-030-89753-6, Softcover ISBN: 978-3-030-89756-7, eBook ISBN: 978-3-030-89754-3.
14. P. Steinleitner, N. Nagl, M. Kowalczyk, *et al.*, "Single-cycle infrared waveform control," Nat. Photonics **16**(7), 512–518 (2022).
15. S. Vasilyev, V. Smolski, J. Peppers, *et al.*, "Middle-IR frequency comb based on Cr:ZnS laser," Opt. Express **27**(24), 35079–35087 (2019).
16. E. Sorokin, N. Tolstik, and I. T. Sorokina, "1 Watt femtosecond mid-IR Cr:ZnS laser," in *Solid State Lasers XXII: Technology and Devices*, vol. 8599 W. A. Clarkson and R. Shori, eds., International Society for Optics and Photonics (SPIE, 2013), p. 859916.
17. N. Tolstik, E. Sorokin, V. Kalashnikov, *et al.*, "Supercontinuum generation in mid-IR using chalcogenide and germanate nonlinear fiber," in *Solid State Lasers XXII: Technology and Devices*, vol. 8599 W. A. Clarkson and R. Shori, eds., International Society for Optics and Photonics (SPIE, 2013), p. 85990K.
18. I. Sorokina, E. Sorokin, S. Mirov, *et al.*, "Continuous-wave tunable Cr2+:ZnS laser," Appl. Phys. B **74**(6), 607–611 (2002).
19. Y. Hu, X. Lu, R. Xu, *et al.*, "Long-term stable, multi-watt direct femtosecond amplification based on cr:zns," Opt. Laser Technol. **188**, 112924 (2025).
20. S. Vasilyev, I. Moskalev, V. Smolski, *et al.*, "27 watt middle-ir femtosecond laser system at 2.4 μm," in *Laser Congress 2018 (ASSL)*, (Optica Publishing Group, 2018), p. AW3A.1.
21. S. Vasilyev, I. S. Moskalev, V. O. Smolski, *et al.*, "Super-octave longwave mid-infrared coherent transients produced by optical rectification of few-cycle 2.5-μm pulses," Optica **6**(1), 111–114 (2019).
22. Z. Wang, A. Abbasi, U. Dave, *et al.*, "Novel light source integration approaches for Silicon photonics," Laser Photonics Rev. **11**(4), 1700063 (2017).
23. I. T. Sorokina, E. Sorokin, S. Mirov, *et al.*, "Broadly tunable compact continuous-wave Cr2+:ZnS laser," Opt. Lett. **27**(12), 1040–1042 (2002).
24. O. L. Hebnes, M. E. Bathen, Ø. S. Schøyen, *et al.*, "Predicting solid state material platforms for quantum technologies," npj Comput. Mater. **8**(1), 207 (2022).
25. J. L. Brinkmann, *Toward a Novel Mid-IR Light Source: Fabrication and Characterization of Cr:ZnS and Silicon Waveguides for Integrated Photonic Applications*, Master Theses (Electrical Engineering) (NTNU/ETH, 2024).
26. C. Brüne, et al., "MBE deposition and spectral-luminescence properties of monocrystalline Cr:ZnS layers on silicon," (2025). Forthcoming.
27. I. T. Sorokina, "Mid-infrared crystalline solid-state lasers," in *Solid-State Mid-Infrared Laser Sources*, I. Sorokina and K. Vodopyanov, eds. (Springer Berlin Heidelberg, 2003), Topics in Applied Physics 89, 557, pp. 255–350.
28. K.-i. Kawamura, M. Hirano, T. Kurobori, *et al.*, "Femtosecond-laser-encoded distributed-feedback color center laser in lithium fluoride single crystals," Appl. Phys. Lett. **84**(3), 311–313 (2004).
29. V. Apostolopoulos, L. Laversenne, T. Colomb, *et al.*, "Femtosecond-irradiation-induced refractive-index changes and channel waveguiding in bulk Ti3+:Sapphire," Appl. Phys. Lett. **85**(7), 1122–1124 (2004).
30. A. G. Okhrimchuk, A. V. Shestakov, I. Khrushchev, *et al.*, "Depressed cladding, buried waveguide laser formed in a YAG:Nd3+ crystal by femtosecond laser writing," Opt. Lett. **30**(17), 2248–2250 (2005).
31. J. R. Macdonald, S. J. Beecher, A. Lancaster, *et al.*, "Compact Cr:ZnS channel waveguide laser operating at 2333 nm," Opt. Express **22**(6), 7052–7057 (2014).
32. Y.-P. Peng, X. Zou, Z. Bai, *et al.*, "Mid-infrared laser emission from cr:zns channel waveguide fabricated by femtosecond laser helical writing," Sci. Rep. **5**(1), 18365 (2015).
33. N. Tolstik, A. G. Okhrimchuk, M. P. Smayev, *et al.*, "Single-mode depressed cladding buried waveguide laser based on single-crystal Cr:ZnS," in *Conference on Lasers and Electro-Optics*, (Optica Publishing Group, 2019), p. STh1E.6.
34. E. Sorokin, A. A. Bushunov, N. Tolstik, *et al.*, "All-laser-microprocessed waveguide Cr:ZnS laser," Opt. Mater. Express **12**(2), 414–420 (2022).
35. J. R. Macdonald, S. J. Beecher, P. A. Berry, *et al.*, "Efficient mid-infrared Cr:ZnSe channel waveguide laser operating at 2486 nm," Opt. Lett. **38**(13), 2194–2196 (2013).
36. S. A. McDaniel, P. A. Berry, K. L. Schepler, *et al.*, "Gain-switched operation of ultrafast laser inscribed waveguides in Cr:ZnSe," in *Solid State Lasers XXIV: Technology and Devices*, vol. 9342 S. A. Clarkson and R. K. Shori, eds., International Society for Optics and Photonics (SPIE, 2015), p. 93420E.
37. S. A. McDaniel, A. Lancaster, J. W. Evans, *et al.*, "Power scaling of ultrafast laser inscribed waveguide lasers in chromium and iron doped zinc selenide," Opt. Express **24**(4), 3502–3512 (2016).
38. P. A. Berry, J. R. Macdonald, S. J. Beecher, *et al.*, "Fabrication and power scaling of a 1.7 W Cr:ZnSe waveguide laser," Opt. Mater. Express **3**(9), 1250–1258 (2013).

Optics EXPRESS

39. A. Lancaster, G. Cook, S. A. McDaniel, *et al.*, "Mid-infrared laser emission from Fe:ZnSe cladding waveguides," Appl. Phys. Lett. **107**(3), 031108 (2015).
40. D. G. Lancaster, S. Gross, H. Ebendorff-Heidepriem, *et al.*, "Fifty percent internal slope efficiency femtosecond direct-written Tm3+:ZBLAN waveguide laser," Opt. Lett. **36**(9), 1587–1589 (2011).
41. F. Thorburn, A. Lancaster, S. McDaniel, *et al.*, "5.9 GHz graphene based q-switched modelocked mid-infrared monolithic waveguide laser," Opt. Express **25**(21), 26166–26174 (2017).
42. S. McDaniel, F. Thorburn, A. Lancaster, *et al.*, "Operation of Ho:YAG ultrafast laser inscribed waveguide lasers," Appl. Opt. **56**(12), 3251–3256 (2017).
43. S. Hakobyan, V. J. Wittwer, K. Hasse, *et al.*, "Highly efficient q-switched Yb:YAG channel waveguide laser with 5.6 W of average output power," Opt. Lett. **41**(20), 4715–4718 (2016).
44. F. E. Thorburn, *Compact high repetition rate mid-infrared solid-state lasers*, Doctoral Theses (Engineering & Physical Sciences) (Heriot-Watt University, 2019).
45. J. Yang, K. V. Gasse, D. M. Lukin, *et al.*, "Titanium:sapphire-on-insulator integrated lasers and amplifiers," Nature **630**(8018), 853–859 (2024).
46. D. Strickland and G. Mourou, "Compression of amplified chirped optical pulses," Opt. Commun. **55**(6), 447–449 (1985).
47. E. Sorokin and I. T. Sorokina, "Femtosecond operation and random quasi-phase-matched self-doubling of ceramic Cr:ZnSe laser," in *Conference on Lasers and Electro-Optics 2010*, (Optica Publishing Group, 2010), p. CTuGG2.
48. A. Rudenkov, V. L. Kalashnikov, E. Sorokin, *et al.*, "High peak power and energy scaling in the mid-IR chirped-pulse oscillator-amplifier laser systems," Opt. Express **31**(11), 17820–17835 (2023).
49. A. Rudenkov, V. Kalashnikov, E. Sorokin, *et al.*, "Roadmap to femtosecond pulse power/energy-scaling in mid-infrared oscillator-amplifier laser systems," in *Conference on Lasers and Electro-Optics/Europe (CLEO/Europe 2023) and European Quantum Electronics Conference (EQEC 2023)*, (Optica Publishing Group, 2023), pp. CA–1.1.
50. M. Demesh, E. Sorokin, E. Einmo, *et al.*, "Depressed cladding buried waveguide lasers: single-crystal vs. polycrystalline Cr:ZnS," in *High-Brightness Sources and Light-Driven Interactions Congress*, (Optica Publishing Group, 2024), p. JW4A.4.
51. S. Vasilyev, M. Mirov, and V. Gapontsev, "Kerr-lens mode-locked femtosecond polycrystalline cr2+:zns and cr2+:znse lasers," Opt. Express **22**(5), 5118–5123 (2014).
52. S. Vasilyev, I. Moskalev, M. Mirov, *et al.*, "Multi-watt mid-ir femtosecond polycrystalline cr2+:zns and cr2+:znse laser amplifiers with the spectrum spanning 2.0–2.6 μm," Opt. Express **24**(2), 1616–1623 (2016).
53. S. Qu, A. Paudel, A. Sebesta, *et al.*, "Directly diode-pumped femtosecond cr:zns amplifier with ultra-low intensity noise," Opt. Lett. **47**(23), 6217–6220 (2022).
54. S. Vasilyev, J. Gu, M. Mirov, *et al.*, "Low-threshold supercontinuum generation in polycrystalline media," J. Opt. Soc. Am. B **38**(5), 1625–1633 (2021).
55. H. R. Telle, G. Steinmeyer, A. E. Dunlop, *et al.*, "Carrier-envelope offset phase control: A novel concept for absolute optical frequency measurement and ultrashort pulse generation," Appl. Phys. B **69**(4), 327–332 (1999).
56. M. Baudrier-Raybaut, R. Haïdar, P. Kupecek, *et al.*, "Random quasi-phase-matching in bulk polycrystalline isotropic nonlinear materials," Nature **432**(7015), 374–376 (2004).
57. S. Ramachandran, J. M. Fini, M. Mermelstein, *et al.*, "Ultra-large effective-area, higher-order mode fibers: a new strategy for high-power lasers," Laser Photonics Rev. **2**(6), 429–448 (2008).
58. F. Stutzki, F. Jansen, H.-J. Otto, *et al.*, "Designing advanced very-large-mode-area fibers for power scaling of fiber-laser systems," Optica **1**(4), 233–242 (2014).
59. M. Demesh, V. L. Kalashnikov, E. Sorokin, *et al.*, "At the threshold of distributed Kerr-lens mode-locking in a Cr: ZnS waveguide laser," J. Opt. Soc. Am. B **40**(7), 1717–1725 (2023).
60. J. Limpert, A. Liem, M. Reich, *et al.*, "Low-nonlinearity single-transverse-mode ytterbium-doped photonic crystal fiber amplifier," Opt. Express **12**(7), 1313–1319 (2004).
61. L. Dong and M. Yasin, "Advanced optical fibers for high power fiber lasers," Advances in optical fiber technology: fundamental optical phenomena and applications pp. 221–252 (2015).
62. E. Einmo, N. Tolstik, C. Grivas, *et al.*, "Morphology characterization and refractive index analysis of subsurface ultrashort-pulsed laser modifications in zns," Physica Status Solidi (a) **221**(17), 2400299 (2024).
63. M. Zitelli, F. Mangini, and S. Wabnitz, "Statistics of modal condensation in nonlinear multimode fibers," Nat. Commun. **15**(1), 1149 (2024).
64. J. Sousa and O. Okhotnikov, "Multimode er-doped fiber for single-transverse-mode amplification," Appl. Phys. Lett. **74**(11), 1528–1530 (1999).
65. Y. Jung, S.-U. Alam, Z. Li, *et al.*, "First demonstration and detailed characterization of a multimode amplifier for space division multiplexed transmission systems," Opt. Express **19**(26), B952–B957 (2011).
66. M. E. Fermann, "Single-mode excitation of multimode fibers with ultrashort pulses," Opt. Lett. **23**(1), 52–54 (1998).
67. A. W. Snyder and J. D. Love, *Optical waveguide theory*, vol. 175 (Chapman and hall London, 1983).
68. K. Krupa, A. Tonello, B. M. Shalaby, *et al.*, "Spatial beam self-cleaning in multimode fibres," Nat. Photonics **11**(4), 237–241 (2017).

138.131.79.212 2025-11-13 09:03:4